

Rotate to Scan: UNet-like Mamba with Triplet SSM Module for Medical Image Segmentation

Hao Tang, Lianglun Cheng, Guoheng Huang, Zhengguang Tan, Junhao Lu and Kaihong Wu

Abstract—Image segmentation holds a vital position in the realms of diagnosis and treatment within the medical domain. Traditional convolutional neural networks (CNNs) and Transformer models have made significant advancements in this realm, but they still encounter challenges because of limited receptive field or high computing complexity. Recently, State Space Models (SSMs), particularly Mamba and its variants, have demonstrated notable performance in the field of vision. However, their feature extraction methods may not be sufficiently effective and retain some redundant structures, leaving room for parameter reduction. In response to these challenges, we introduce a methodology called Triplet Mamba-UNet, characterized by Residual VSS Block and Triplet SSM Module. The Residual VSS block is devised to mitigate the onset of network degradation caused by the diminishing efficacy of information transfer from shallower to deeper layers. Meanwhile, the Triplet SSM Module is devised to tackle the challenges associated with spatial feature extraction within State Space Models. We conducted experiments on ISIC17, ISIC18, CVC-300, CVC-ClinicDB, Kvasir-SEG, CVC-ColonDB and Kvasir-Instrument datasets, demonstrating the superior segmentation performance of our proposed TM-UNet. Additionally, compared to the previous VM-UNet, our model achieves a one-third reduction in parameters.

Index Terms—U-Net, State Space Models, Medical image segmentation, Mamba

I. INTRODUCTION

AUTOMATIC medical image segmentation plays a crucial role in disease diagnosis and surgery, which enables clinicians to accurately delineate anatomical structures, identify abnormalities, and plan surgical interventions with precision and efficiency [1]. Over the years, deep learning-based segmentation methods have performed remarkably, leveraging CNNs [2] and Transformer [3] as the cornerstone architecture. Among these, U-Net [4], renowned for its efficacy in segmenting medical images, has garnered widespread adoption and adaptation within the realm of medical imaging.

The U-shaped architecture stands as a pivotal framework lauded for its harmonious Encoder-Decoder design coupled

with the integration of skip connections. It employs a hierarchical approach, utilizing multiple encoding layers to progressively extract features and transform high-dimensional images into low-dimensional representations. Meanwhile, symmetric decoding layers are used to decode these features gradually and map them back to high-dimensional space. Furthermore, the integration of skip connections facilitates the fusion of features from different hierarchical levels with their corresponding decoding layers, thereby enhancing the model's ability to capture fine-grained details and contextual information. Hence, a plethora of U-shaped architectures have begun to emerge. Initially, most researchers focused on modifications atop CNNs. However, due to the limited receptive fields of CNNs [5]–[7], which predominantly attend to local features, they failed to model long-range dependencies effectively, yielding marginal improvements. It was not until the advent of TransUNet [8] that the integration of Transformer architecture within the U-shaped framework occurred, endowing encoders with the capability to capture long-distance information. The Medical Transformer [9] introduced a novel approach by utilizing consecutive Transformer blocks as encoders and employing a patch-to-image training strategy, achieving results surpassing those obtained by pure convolutional methods. SwinUNet [10] represents the first U-shaped architecture solely based on Transformers, surpassing the segmentation accuracy of both pure convolutional and hybrid Transformer-convolution models. Furthermore, the U-shaped architecture has spawned several derivative models such as UNETR [11], DS-TransUNet [12], and nnFormer [13].

Another issue has surfaced with the widespread integration of Transformers: the substantial increase in computational complexity due to attention mechanisms, resulting in escalated model parameter counts and consequently prolonged inference and training times [14]. To address this issue, Gu et al. initially introduced S4 (Structured State Space Sequence Models) [15], offering a solution for modeling long-range dependencies in sequences within limited storage capacity. Building upon this groundwork, they extended the approach by proposing S6 (S4 models with a selection mechanism and computed with a scan) and integrated it into an end-to-end neural network, resulting in Mamba [16]. Mamba showcases rapid inference, with a throughput five times higher than that of Transformers, and demonstrates linear scaling in sequence length. VisionMamba [17] and VMamba [18] were the first to apply Mamba in computer vision. They respectively conducted selective scans on image patches in two and four directions, achieving performance comparable to Swin Transformer [19] while signifi-

This paragraph of the first footnote will contain the date on which you submitted your paper for review. It will also contain support information, including sponsor and financial support acknowledgment. For example, "This work was supported in part by the U.S. Department of Commerce under Grant BS123456."

Hao Tang, Lianglun Cheng, Guoheng Huang, Zhengguang Tan, Junhao Lu and Kaihong Wu are with the School of Computer Science and Technology, Guangdong University of Technology, Guangzhou 510006, China (e-mail: t1770134538@outlook.com; llcheng@gdut.edu.cn; kevin-wong@gdut.edu.cn; bcbillycat@qq.com; polynya-code@outlook.com; zhexuejia123456@outlook.com).

cantly reducing time complexity. Subsequently, Mamba was integrated into U-shaped architectures [20]–[22], showcasing its competitiveness. Yet, these approaches lack methods akin to spatial attention mechanisms, thus only accounting for encoding inter-channel information but disregarding the significance of spatial information, let alone efficiently fusing channel features with spatial features. Additionally, despite the significantly reduced parameter count of these Mamba-based U-shaped architecture methods compared to Transformer-based approaches, there remains room for optimization. In fact, the current Mamba-based methods are characterized by some redundant modules within the encoder and decoder. This redundancy suggests that there is potential for the parameter quantity to be further diminished, an adjustment that would render the methodology suitable for deployment on lightweight devices.

In response to the challenges above, in this paper, we propose a lightweight module named Triplet SSM, incorporated into our proposed model Triplet Mamba UNet (TM-UNet). The Triplet SSM leverages the selective scan operation inherent in SSM to efficiently learn spatial relevant features. Diverging from conventional attention mechanisms, which often entail many additional learnable parameters, the Triplet SSM explores strategies for constructing cost-effective yet impactful attention-like mechanisms while ensuring comparable or superior performance. Our focus lies in emphasizing the significance of capturing cross-dimensional interactions when performing selective scan operations, thereby facilitating the generation of comprehensive feature representations. Specifically, the proposed Triplet SSM exploits three selective scan operations to aggregate features of the input tensor in different directions. One operates along the original channel direction, while the other two operate along the vertical and horizontal directions, respectively. The three resulting feature maps then undergo further fusion via simple gating units.

In order to cut down the parameter count, unlike previous Mamba-based methods, we use fewer VSS blocks employed in the encoder, thereby minimizing redundant operations. Furthermore, we adopt two VSS blocks and one Triplet SSM module as the bottleneck part, thus increasing the interaction of information across different dimensions, resulting in a reduction of parameters to two-thirds of the VM-UNet and four-fifths of the VM-UNetV2 while enhancing segmentation performance. Furthermore, we present the ResVSS block, an extension of the VSS block derived from VMamba, wherein residual connections are added at both ends. This augmentation facilitates the integration of a mechanism aimed at sharing global and local feature states to enhance performance, particularly on detailed images.

In summary, our main contributions are as follows:

- We present an innovative U-shaped Mamba model denoted as TM-UNet, integrating the Triplet SSM, VSS block and ResVSS block. This integration reduces parameters while concurrently strengthening segmentation accuracy.
- To tackle the challenge of fusing spatial and channel features, we propose the lightweight feature fusion module, Triplet SSM, which to the best of our knowledge, is the first

attempt to use pure SSM to integrate spatial and channel features.

- To address the issue of excessive parameters, we reduce the utilization of VSS blocks, thereby minimizing redundant structures. Then, we propose the ResVSS block, which enhances the capability of the VSS block to capture local and global features more comprehensively through residual connections.
- We conducted multiple experiments, resulting in a reduction in parameters and an increase in mIOU from 78.82% to 80.51% on the ISIC17 dataset and from 79.39% to 81.55% on the ISIC18 dataset compared to previous Mamba methods.

II. RELATED WORK

The fusion of spatial-wise and channel-wise features has been a focal point in the advancement of medical image segmentation models, aiming to enhance the understanding of complex anatomical structures and abnormalities. Convolutional Block Attention Module (CBAM) [23] is the pioneering framework that integrates spatial and channel features. It comprises two primary components: the Channel Attention Module (CAM) and the Spatial Attention Module (SAM). The CAM recalibrates feature maps by capturing inter-channel dependencies, emphasizing channel-wise importance. Conversely, the SAM attends to informative spatial regions within feature maps, thereby focusing on intra-channel dependencies. DANet [24], unlike traditional methods that consider only local or global relationships, captures the interdependencies between any two positions in a feature map, allowing features from similar positions to contribute to each other’s enhancement regardless of their distance. Coordinate attention [25] improves spatial awareness in neural networks by focusing on horizontal and vertical relationships within feature maps. By capturing feature distributions along each axis and compressing the information, it enhances spatial understanding without overwhelming the model with unnecessary technical complexity. The Bottleneck Attention Module (BAM) [26], similar to CBAM, seamlessly incorporates Channel and Spatial Attention Mechanisms to adaptively adjust channel feature responses, thereby accentuating both global and local information. After assimilating the characteristics of previous methods, Misra et al. introduced Triplet Attention [27], which employs a three-branch structure to capture cross-dimensional interactions for computing attention weights. For input tensors, Triplet Attention applies rotational operations followed by residual transformations to establish inter-dependencies among dimensions, encoding information across channels and spatial dimensions with negligible computational overhead. Moreover, in contrast to prior methods, Triplet Attention underscores the importance of multidimensional interactions without dimensionality reduction, thereby eliminating indirect correspondences between channels and weights. This renders Triplet Attention an efficient approach and inspires the present work.

III. METHODOLOGY

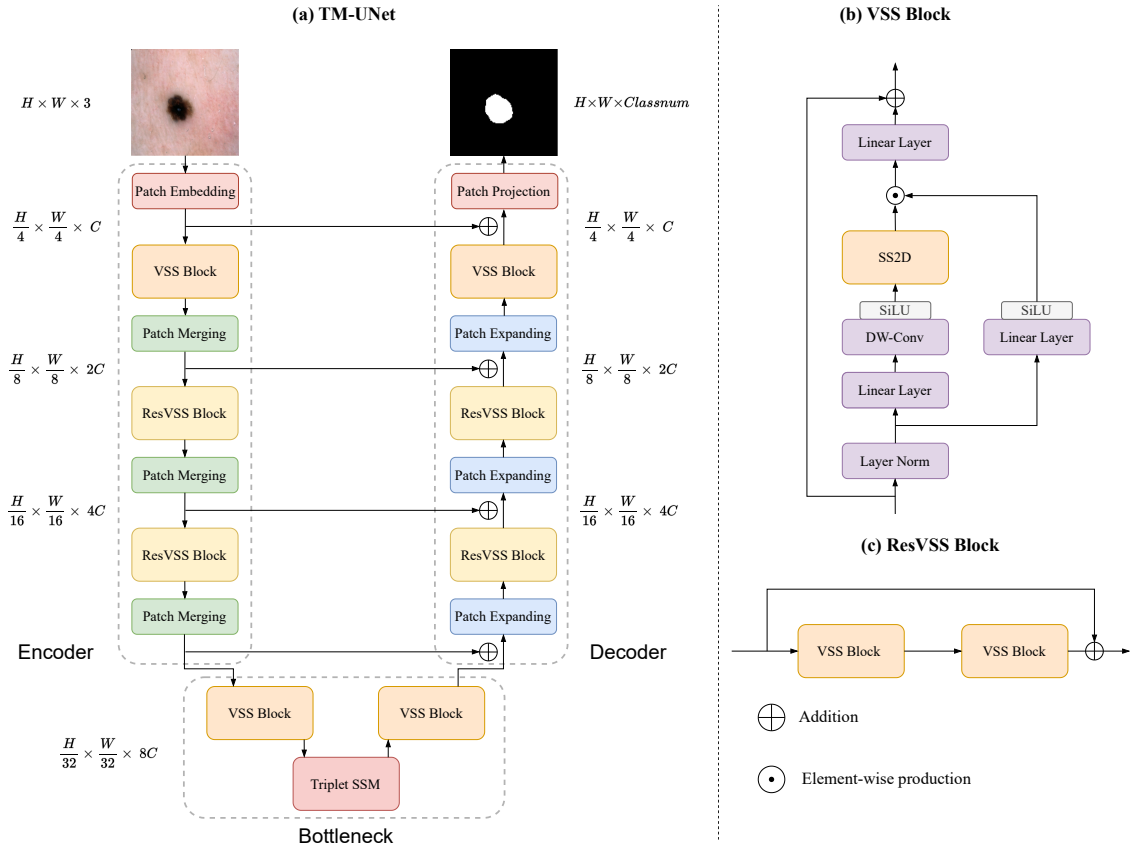


Fig. 1. (a) The overall architecture of our proposed TM-UNet, following the encoder, bottleneck, and decoder structure design. (b) The Vision State Space (VSS) block serves as the backbone of VM-UNet, with the SS2D operation constituting its core functionality. (c) ResVSS block comprises two consecutive VSS blocks, featuring a skip connection from the beginning to the end.

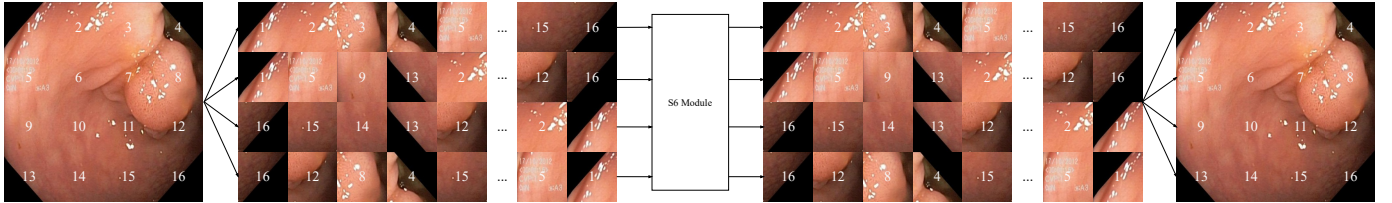


Fig. 2. The operations in the SS2D derived from Vmamba, which consists of scan expanding, S6 feature extraction, and scan merging.

A. Preliminary

In contemporary SSM-based models, such as S4 and Mamba, reliance is placed on a conventional continuous system. This system maps a one-dimensional input function or sequence, denoted as $x(t) \in \mathbb{R}$, through intermediary implicit states $h(t) \in \mathbb{R}^N$ to an output $y(t) \in \mathbb{R}$. This mapping process can be illustrated as a linear Ordinary Differential Equation (ODE):

$$\begin{aligned} h'(t) &= Ah(t) + Bx(t) \\ y(t) &= Ch(t) \end{aligned} \quad (1)$$

In this equation, $A \in \mathbb{R}^{N \times N}$ represents the state matrix, while $B \in \mathbb{R}^{N \times 1}$ and $C \in \mathbb{R}^{N \times 1}$ denote the projection parameters.

S4 and Mamba discretize this continuous system to suit deep learning contexts better. They introduce a timescale parameter Δ and convert A and B into discrete parameters \bar{A} and \bar{B} using a consistent discretization rule. The zero-order hold (ZOH)

method is typically employed for discretization, outlined as follows:

$$\begin{aligned} \bar{A} &= \exp(\Delta A) \\ \bar{B} &= (\Delta A)^{-1}(\exp(\Delta A) - I) \cdot \Delta B \end{aligned} \quad (2)$$

After discretization, SSM-based models can be computed using two distinct methods: linear recurrence or global convolution, denoted as equations (3) and (4).

$$\begin{aligned} h'(t) &= \bar{A}h(t) + \bar{B}x(t) \\ y(t) &= Ch(t) \end{aligned} \quad (3)$$

$$\begin{aligned} \bar{K} &= (C\bar{B}, C\bar{A}\bar{B}, \dots, C\bar{A}^{L-1}\bar{B}) \\ y &= x * \bar{K} \end{aligned} \quad (4)$$

Where $\bar{K} \in \mathbb{R}^L$ represents a structured convolutional kernel, and L denotes the length of the input sequence x .

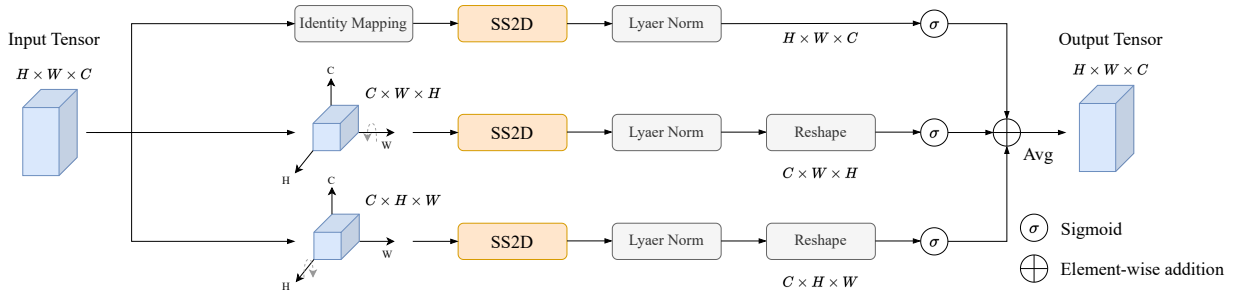


Fig. 3. Illustration of our proposed Triplet SSM, comprising three branches. The upper branch extracts the channel feature of the input tensor. The middle branch captures spatial information across channel dimension C and width dimension W . The lowest branch handles the height dimension H and the channel dimension C .

B. Overview of the TM-UNet

The overall architecture of TM-UNet, illustrated in Fig. 1 (a), embraces a symmetrical design comprising patch embedding, encoder, bottleneck, decoder, and final patch projection. Given an input image $x \in \mathbb{R}^{H \times W \times 3}$, the patch embedding layer amalgamates every non-overlapping 4×4 pixel region into an image patch and projects its channel dimension to C . This operation results in a processed feature map reshaping to $\frac{h}{4} \times \frac{w}{4} \times C$, where h and w denote the height and width of the input image, respectively. Such transformation facilitates efficient representation of local image information while reducing computational complexity. Subsequently, the feature map undergoes feature extraction through four stages of VSS blocks. Here, the VSS blocks maintain the shape of the feature map but, via the patch merging module, reduce the height and width by half with each pass while doubling the number of channels. Consequently, the output shape of each stage within the encoder progresses sequentially as $\frac{H}{4} \times \frac{W}{4} \times C$, $\frac{H}{8} \times \frac{W}{8} \times 2C$, $\frac{H}{16} \times \frac{W}{16} \times 4C$, and $\frac{H}{32} \times \frac{W}{32} \times 8C$. The features are fed into the decoder following two VSS blocks and the Triplet SSM as the bottleneck part. The shape transformation in the decoder is conversely executed, with the final patch projection module, consisting of patch expanding operation and a linear projection layer, projecting the shape $\frac{H}{4} \times \frac{W}{4} \times C$ to $H \times W \times Classnum$.

Before each VSS block in the encoder, a skip connection is established to connect with the corresponding location in the decoder. These skip connections facilitate the propagation of information from earlier encoder stages to later decoder stages, aiding in preserving and utilizing low-level features throughout the network.

C. VSS Block and ResVSS Block

The VSS block, originating from VMamba and serving as the backbone of the TM-UNet encoder and decoder, is depicted in Fig. 1(b). Initially, the input undergoes processing through an initial linear embedding layer, following which it branches into two separate information streams. One stream undergoes a 3×3 depth-wise convolution [28] layer and subsequently a Silu activation [28] function before entering the main 2D-Selective-Scan (SS2D) module. The SS2D operation comprises scan expanding, S6 block [16] feature extraction, and scan merging operations. As depicted in Fig. 2, the scan expanding operation divides the image patch into four sequences

based on four directions. Following this, these four sequences undergo feature extraction via the S6 block. Compared to Vision Mamba’s two-directional scanning, this approach enables a more comprehensive learning of information. Finally, the feature map obtained from the S6 block is restored to its original shape through scan merging.

The output of the SS2D module then passes through a layer normalization and is combined with the output from the other information stream, which has also undergone Silu activation. The merged output constitutes the final result of the VSS block. The following formula can represent the process of the VSSBlock:

$$\begin{aligned} \hat{x} &= \alpha_1(\gamma(x)) \\ \hat{y} &= \alpha_2(\sigma_1(\psi(W * \hat{x} + b)) \otimes \sigma_2(\hat{x})) + x \end{aligned} \quad (5)$$

Where γ denotes layer normalization, α represents the linear layer, W and b signify the kernel and bias in Depthwise Convolution respectively, σ indicates the SiLU activation function, \otimes denotes element-wise multiplication, and ψ represents the SSM operations. Given an input tensor $X = [x_1, x_2, \dots, x_c]$, the output transformed tensor from VSS block $Y = [\hat{y}_1, \hat{y}_2, \dots, \hat{y}_c]$ retains the same size of X .

Building upon the foundation of the VSS block, we present an evolved variant: the ResVSS block, shown in Fig. 1(c). A residual connection is established that initiates a route from the input of the first VSS block and terminates at the output of the second VSS block. This enables the element-wise addition of the original information unaffected by the VSS block to the transformed information processed by the VSS block, promoting efficiency and richness of information transfer from the shallower network layers to the deeper ones, particularly by capitalizing on identity mapping. The ResVSS block mitigates the degradation issues arising from stacking original VSS blocks while avoiding the introduction of additional learnable parameters. The process is defined as follows:

$$y = \text{VSS}_1(\text{VSS}_2(x)) + x \quad (6)$$

Here, x and y are the input and output tensors, VSS_1 and VSS_2 denote the first VSS block and the second.

D. Triplet SSM

Our TripletSSM module accepts an input tensor $z \in \mathbb{R}^{H \times W \times C}$ and produces an output tensor $Z \in \mathbb{R}^{H \times W \times C}$. This process

TABLE I

QUANTITATIVE COMPARISON BETWEEN TM-UNET AND OTHER METHODS FOR ISIC 2017 AND ISIC 2018(BOLD INDICATES THE BEST, UNDERLINE INDICATES THE SECOND BEST.)

Dataset	Model	mIoU(%) \uparrow	DSC(%) \uparrow	Acc(%) \uparrow	Spe(%) \uparrow	Sen(%) \uparrow
ISIC17	UNet	74.94	85.68	95.33	97.72	83.44
	UNet++ [29]	75.44	86.00	95.35	97.34	85.40
	Att-UNet [30]	76.17	86.47	95.49	97.40	86.02
	UTNetV2 [31]	78.19	87.76	95.94	97.72	87.07
	UNetV2 [32]	77.53	87.34	95.76	97.44	87.41
	TransFuse [33]	77.00	87.00	95.68	97.55	86.35
	C ² SGD [34]	76.83	86.70	95.68	97.74	85.44
	Att-Swin UNet [35]	76.32	86.28	94.15	95.66	89.44
	VM-UNet	77.88	87.92	95.73	97.96	85.68
	VM-UNetV2	78.82	88.15	94.14	95.66	89.43
	TM-UNet (Proposed)	80.51	89.20	96.46	98.28	87.37
ISIC18	UNet	77.83	87.70	94.26	97.56	84.02
	UNet++ [29]	78.31	87.83	94.02	95.75	88.65
	Att-UNet [30]	77.23	87.16	93.93	<u>96.93</u>	84.61
	UTNetV2 [31]	78.97	<u>88.25</u>	<u>94.32</u>	96.48	87.6
	UNetV2 [32]	78.32	<u>87.84</u>	<u>94.18</u>	96.69	86.39
	TransFuse [33]	78.22	87.78	94.10	96.39	87.00
	C ² SGD [34]	78.13	87.72	94.11	96.58	86.25
	Att-Swin UNet [35]	78.32	87.99	93.91	95.37	89.33
	VM-UNet	78.82	88.15	94.15	95.66	<u>89.44</u>
	VM-UNetV2	<u>79.39</u>	87.88	94.16	96.51	86.89
	TM-UNet (Proposed)	81.55	89.84	95.08	96.68	89.98

involves three separate branches, whose specifics are delineated in Fig. 3. In the first branch, no transformation is applied to the tensor. Instead, it undergoes the SS2D module. This branch aims to capture channel features independent of spatial information. The tensor is rotated 90 degrees clockwise along the W-axis in the second branch, denoted as $z_1^* \in R^{C \times W \times H}$. Subsequently, SS2D operations are performed, extracting features from the channel and H dimensions and establishing spatial correlations. The third branch takes a similar approach but the tensor is rotated 90 degrees counterclockwise along the H-axis, denoted as $z_2^* \in R^{C \times W \times H}$. SS2D operations are then applied to extract features from the channel and W dimensions. The second and third branches extract features along two directions, yielding two spatially aware feature maps. Additionally, owing to SSM's characteristics, we are able to model long-range information from both directions. Following each SSM operation, layer normalization is implemented coupled with a sigmoid function. The tensors obtained from z_1 and z_2 are reshaped to their initial shapes for element-wise addition with the tensor obtained from z denoted as z_3 , followed by averaging to yield the final output tensor, maintaining the same shape as the input.

In general, all operations of the Triplet SSM can be represented by the following equations:

$$Z = \frac{1}{3} (\sigma_1(\gamma_1(\psi_1(z_1^*))) + \sigma_2(\gamma_2(\psi_2(z_2^*))) + \sigma_3(\gamma_3(\psi_3(z_3)))) \quad (7)$$

Where the ψ represents the SSM operations; γ represents layer normalization, and the σ represents the sigmoid activation function, utilized for learning the weights of each feature in the final output tensor. The equation can be further simplified to

equation (8):

$$Z = \frac{1}{3} (\overline{Z_1} + \overline{Z_2} + Z_3) \quad (8)$$

Here, $\overline{Z_1}$ and $\overline{Z_2}$ represent the outputs from SS2D after the reshape operation.

Apart from the SS2D module, the Triplet SSM does not employ linear or convolutional layers, nor does it involve multiplication operations. Therefore, the computational cost associated with this module is relatively low. Furthermore, the introduction of spatial-related information enables the model to acquire more comprehensive knowledge, leading to improved performance in instance segmentation metrics, as detailed in the ablation experiments section.

E. Loss function

Since the image masks utilized in our medical image segmentation are binary, the segmentation task can be regarded as a pixel-wise binary classification. Hence, we employ a combination of Binary Cross Entropy and DICE loss as the overall loss function, as represented in equations (9)-(11).

$$L_{Bce} = -\frac{1}{N} \sum_1^N [y_i \log(\hat{y}_i) + (1 - y_i) \log(1 - \hat{y}_i)] \quad (9)$$

$$L_{Dice} = 1 - \frac{2|X \cap Y|}{|X| + |Y|} \quad (10)$$

$$L_{BceDice} = \lambda_1 L_{Bce} + \lambda_2 L_{Dice} \quad (11)$$

where N denotes the total number of samples. y_i represents the ground truth and \hat{y}_i represents the predicted value. $|X|$ and $|Y|$ denote the predicted values and ground truth, respectively. ϕ_1 and ϕ_2 are both trial values typically set to 1.

TABLE II

COMPARATIVE EXPERIMENTAL RESULTS ON THE KVASIR-INSTRUMENT, KVASIR-SEG, CLINICDB, COLONDB, AND CVC-300 DATASETS(BOLD INDICATES THE BEST, UNDERLINE INDICATES THE SECOND BEST)

Dataset	Model	mIoU(%) \uparrow	DSC(%) \uparrow	Acc(%) \uparrow	Spe(%) \uparrow	Sen(%) \uparrow
Kvasir-Instrument	UNet	87.74	93.47	98.78	99.33	93.45
	UNet++	<u>90.01</u>	94.48	<u>99.01</u>	99.48	94.78
	Att-UNet	88.90	94.12	98.91	<u>99.54</u>	92.89
	UTNetV2	86.91	92.99	98.71	<u>99.41</u>	91.67
	UNetV2	89.07	94.22	98.93	99.52	93.24
	Transfuse	89.77	<u>94.61</u>	99.00	99.51	<u>94.02</u>
	C ² SGD	89.70	94.57	98.99	99.53	93.77
	Att-Swin UNet	89.11	94.02	99.01	99.42	93.88
	VM-UNet	88.67	93.99	98.90	99.55	92.51
	VM-UNetV2	87.30	93.22	98.75	99.41	92.33
	TM-UNet (Proposed)	90.12	94.68	99.04	99.56	93.68
Kvasir-SEG	UNet	72.46	84.03	95.32	97.65	82.12
	UNet++	76.17	86.48	96.11	98.44	82.89
	Att-UNet	76.05	86.39	96.17	<u>98.83</u>	81.09
	UTNetV2	77.15	87.10	96.33	98.64	82.59
	UNetV2	<u>77.67</u>	87.50	96.31	98.55	83.70
	Transfuse	68.82	81.53	94.81	98.07	76.34
	C ² SGD	77.80	87.32	96.28	98.33	84.57
	Att-Swin UNet	75.63	86.16	94.61	97.81	83.16
	VM-UNet	78.66	88.05	96.61	98.96	83.27
	VM-UNetV2	76.99	87.00	96.12	97.81	86.55
	TM-UNet (Proposed)	<u>77.83</u>	<u>87.53</u>	<u>96.37</u>	98.37	<u>85.02</u>
ClinicDB	UNet	78.60	88.02	98.13	99.19	85.92
	UNet++	83.24	90.86	98.59	99.53	87.66
	Att-UNet	79.46	88.55	98.26	<u>99.50</u>	84.00
	UTNetV2	80.78	89.37	98.38	99.50	85.42
	UNetV2	77.75	87.49	98.06	99.21	84.79
	Transfuse	71.59	83.44	97.51	99.14	78.69
	C ² SGD	83.30	91.01	97.71	99.17	91.06
	Att-Swin UNet	79.66	88.68	98.22	99.18	87.22
	VM-UNet	76.53	86.71	97.92	99.05	84.89
	VM-UNetV2	<u>83.80</u>	<u>91.19</u>	<u>98.59</u>	99.22	91.35
	TM-UNet (Proposed)	83.82	91.20	98.59	99.25	<u>91.10</u>
ColonDB	UNet	42.41	59.56	94.60	97.91	53.40
	UNet++	44.62	64.71	95.42	99.11	49.58
	Att-UNet	47.86	64.73	95.76	99.26	52.27
	UTNetV2	50.48	67.09	94.57	96.19	<u>74.34</u>
	UNetV2	51.33	67.84	95.22	97.45	67.62
	Transfuse	46.08	63.09	94.50	97.02	63.14
	C ² SGD	<u>55.03</u>	<u>70.99</u>	<u>95.70</u>	<u>97.73</u>	70.58
	Att-Swin UNet	52.35	68.51	93.92	96.38	65.38
	VM-UNet	51.17	67.70	95.55	98.19	62.67
	VM-UNetV2	51.89	68.32	95.31	97.52	67.85
	TM-UNet (Proposed)	57.23	72.80	96.26	98.58	98.37
CVC-300	UNet	67.15	80.35	98.55	98.90	88.22
	UNet++	71.82	83.60	98.89	99.40	84.30
	Att-UNet	<u>76.10</u>	<u>86.07</u>	98.07	99.28	93.07
	UTNetV2	64.55	78.46	98.31	98.53	91.80
	UNetV2	70.35	82.60	98.71	98.97	91.19
	Transfuse	72.88	84.31	<u>98.89</u>	99.23	88.95
	C ² SGD	63.50	77.72	98.22	98.43	92.23
	Att-Swin UNet	66.77	80.07	98.53	98.91	87.66
	VM-UNet	68.57	81.35	98.68	99.12	85.89
	VM-UNetV2	72.30	83.92	98.81	99.03	92.51
	TM-UNet (Proposed)	77.79	87.51	99.11	<u>99.32</u>	<u>92.94</u>

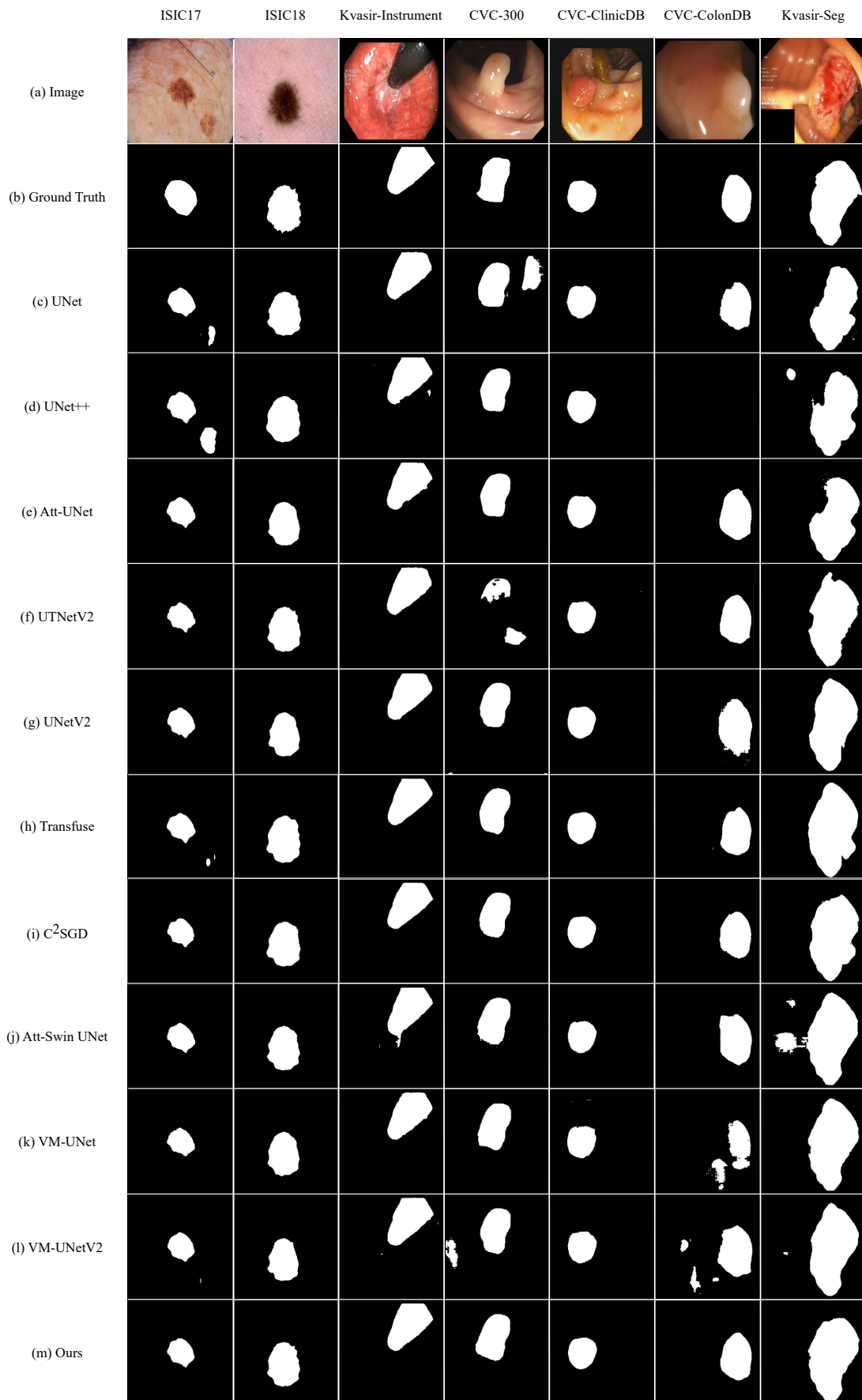


Fig. 4. Visual comparison of segmentation results for Table I and Table II. The top text in the image represents the dataset, while the left text represents their corresponding groups.

TABLE III
FLOPS AND PARAMS COMPARISONS(BOLD INDICATES THE BEST)

Model	UNet	UNet++	Att-UNet	UTNetV2	UNetV2	Transfuse	C ² SGD	Att-Swin UNet	VM-UNet	VM-UNetV2	TM-UNet
Flops(G)↓	54.73	199.64	66.63	17.25	3.90	8.64	7.97	8.69	4.73	4.40	3.42
Params(M)↓	31.03	47.18	34.88	10.02	24.90	26.25	22.00	46.90	27.50	22.77	18.41

TABLE IV
ABLATION STUDIES ON TRIPLET SSM MODULE AND RESIDUAL CONNECTION(BOLD INDICATES THE BEST)

Datasets	configurations	Params(M)↓	mIoU(%)↑	DSC(%)↑	Acc(%)↑	Spe(%)↑	Sen(%)↑
ISIC17	(a)	18.41	76.51	85.77	94.43	97.08	84.69
	(b)	18.41	79.89	88.82	96.27	97.84	88.49
	(c)	18.41	80.51	89.20	96.46	98.28	87.37
ISIC18	(a)	18.41	77.56	87.36	93.68	94.99	88.90
	(b)	18.41	81.01	89.51	94.92	96.79	89.09
	(c)	18.41	81.55	89.84	95.08	96.68	89.98
Kvasir-Instrument	(a)	18.41	87.40	93.28	98.75	99.38	92.71
	(b)	18.41	89.58	94.51	98.99	99.56	93.46
	(c)	18.41	90.12	94.68	99.04	99.56	93.68

IV. EXPERIMENTS

We conducted extensive experiments on the TM-UNet, employing datasets covering skin lesions, intestinal polyps, and surgical instrument segmentation.

A. Datasets

ISIC17 [36] and ISIC18 [37] datasets are two extensive collections of dermoscopic images developed by the International Skin Imaging Collaboration (ISIC), aimed at aiding researchers in devising image analysis tools for the automated diagnosis of melanoma from dermoscopic images. The ISIC17 dataset comprises 2150 images, while ISIC18 includes 2694 images, with a partitioning of these images into training and validation sets at a 7:3 ratio.

Concerning the polyp dataset, we employed five publicly available datasets. Our training set follows the configuration in [38], which consists of 900 images from Kvasir-SEG [39] and 550 images from CVC-ClinicDB [40], totaling 1450 samples. The test set comprises four subsets: the remaining 100 images from Kvasir-SEG, the remaining 62 images from CVC-ClinicDB, the complete CVC-ColonDB [41] dataset comprising 380 samples, and 60 from the CVC-300 [42] dataset.

Additionally, we utilized the Kvasir instrument dataset [43], designed specifically for medical instrument segmentation in gastrointestinal surgery.

B. Implementation Details

The model was trained on a system running Ubuntu 22.04.3, with Python 3.8, CUDA 11.8, and an RTX 4090 GPU (24GB). Before feeding the images into the model, we resized them to 256x256 and applied random flipping and rotation operations for data augmentation. We employed the AdamW [44] optimizer with an initial learning rate of 1e-3, along with the CosineAnnealingLR [45] scheduler, with a maximum of 50 iterations and a minimum learning rate of 1e-5. The VMamba-S pre-trained weights were utilized as the initial weights for the TM-UNet

encoder and decoder. We maintained a uniform batch size of 32 for all datasets used and trained for 300 epochs.

C. Comparison Results

We compared TM-UNet with several existing methods. As shown in Table I, our approach demonstrated superior performance over the previous state-of-the-art models VM-UNetV2, across various metrics including mIoU, DSC, and Acc on the ISIC17 and ISIC18 datasets. Moreover, according to Table II, our approach showcases performance on par with or exceeding that of other models during comparative analysis. Notably, it exhibited noteworthy advancements over VM-UNet and VM-UNetV2 on the polyp and Kvasir instrument datasets, particularly in the ColonDB and CVC-300 datasets, which brought improvement up to 6.54% and 5.49% respectively. The visualized results are presented in Fig. 4, indicating that our model performs better than others.

Furthermore, we also compared the FLOPs (Floating point operations) and parameter counts of the models, as detailed in Table III. When the input size of the models was fixed at (3,256,256), our method exhibited the fewest floating point operations and had nearly one-third fewer parameters than VM-UNet, reducing memory and storage consumption significantly.

D. Ablation Study

To investigate the effectiveness of the ResVSS block and Triplet SSM, we conducted ablation experiments on the ISIC 2017, ISIC 2018, and Kvasir-Instrument datasets. The models in the experiment were configured as follows: (a) a modified U-shaped Mamba UNet serves as the baseline, with 1, 2, and 2 VSS blocks in each stage of the encoder, and 2 VSS blocks in the bottleneck. In the decoder, each stage contains 2, 2, and 1 VSS blocks, respectively; (b) integration of Triplet SSM into the baseline’s bottleneck section; and (c) addition of residual connections before and after the encoder and decoder with a depth of 2, forming the proposed TM-UNet.

From Table IV, it is evident that the proposed ResVSS block and Triplet SSM in this study almost incur no increase in parameter count while significantly improving mIoU and DSC, which validates the proposed approach's effectiveness.

V. CONCLUSION

In this paper, we propose a pure SSM-based U-shaped architecture model, TM-UNet, utilizing residual VSS blocks as the encoder and decoder, and Triplet SSM as the bottleneck. Extensive experimental results demonstrate that TM-UNet exhibits superior performance compared to previous SSM-based U-shaped models with fewer parameters. Future directions include delving into weakly supervised learning methodologies and further parameter reduction, thereby mitigating training data and computational resource demands. Our ultimate objective is to facilitate the widespread deployment of TM-UNet across diverse application domains.

REFERENCES

- [1] J.-Z. Cheng, D. Ni, Y.-H. Chou, J. Qin, C.-M. Tiu, Y.-C. Chang, C.-S. Huang, D. Shen, and C.-M. Chen, "Computer-aided diagnosis with deep learning architecture: Applications to breast lesions in us images and pulmonary nodules in ct scans," *Scientific Reports*, vol. 6, 2016.
- [2] Y. LeCun and Y. Bengio, *Convolutional networks for images, speech, and time series*, p. 255–258. Cambridge, MA, USA: MIT Press, 1998.
- [3] O. Ronneberger, P. Fischer, and T. Brox, "U-net: Convolutional networks for biomedical image segmentation," in *Medical Image Computing and Computer-Assisted Intervention – MICCAI 2015* (N. Navab, J. Hornegger, W. M. Wells, and A. F. Frangi, eds.), (Cham), pp. 234–241, Springer International Publishing, 2015.
- [4] A. Vaswani, N. M. Shazeer, N. Parmar, J. Uszkoreit, L. Jones, A. N. Gomez, L. Kaiser, and I. Polosukhin, "Attention is all you need," in *Neural Information Processing Systems*, 2017.
- [5] X. Xiao, S. Lian, Z. Luo, and S. Li, "Weighted res-unet for high-quality retina vessel segmentation," in *2018 9th International Conference on Information Technology in Medicine and Education (ITME)*, pp. 327–331, 2018.
- [6] S. Guan, A. A. Khan, S. Sikdar, and P. V. Chitnis, "Fully dense unet for 2-d sparse photoacoustic tomography artifact removal," *IEEE Journal of Biomedical and Health Informatics*, vol. 24, pp. 568–576, 2018.
- [7] N. Ibtehaz and M. S. Rahman, "MultiResUNet : Rethinking the U-Net architecture for multimodal biomedical image segmentation," *Neural Netw.*, vol. 121, pp. 74–87, Jan 2020.
- [8] J. Chen, Y. Lu, Q. Yu, X. Luo, E. Adeli, Y. Wang, L. Lu, A. L. Yuille, and Y. Zhou, "Transunet: Transformers make strong encoders for medical image segmentation," *ArXiv*, vol. abs/2102.04306, 2021.
- [9] J. M. J. Valanarasu, P. Oza, I. Hacıhaliloglu, and V. M. Patel, "Medical transformer: Gated axial-attention for medical image segmentation," in *Medical Image Computing and Computer Assisted Intervention – MICCAI 2021* (M. de Bruijne, P. C. Cattin, S. Cotin, N. Padoy, S. Speidel, Y. Zheng, and C. Essert, eds.), (Cham), pp. 36–46, Springer International Publishing, 2021.
- [10] H. Cao, Y. Wang, J. Chen, D. Jiang, X. Zhang, Q. Tian, and M. Wang, "Swin-unet: Unet-like pure transformer for medical image segmentation," in *Computer Vision – ECCV 2022 Workshops* (L. Karlinsky, T. Michaeli, and K. Nishino, eds.), (Cham), pp. 205–218, Springer Nature Switzerland, 2023.
- [11] A. Hatamizadeh, Y. Tang, V. Nath, D. Yang, A. Myronenko, B. Landman, H. R. Roth, and D. Xu, "Unetr: Transformers for 3d medical image segmentation," in *2022 IEEE/CVF Winter Conference on Applications of Computer Vision (WACV)*, (Los Alamitos, CA, USA), pp. 1748–1758, IEEE Computer Society, jan 2022.
- [12] A. Lin, B. Chen, J. Xu, Z. Zhang, G. Lu, and D. Zhang, "Ds-transunet: Dual swin transformer u-net for medical image segmentation," *IEEE Transactions on Instrumentation and Measurement*, vol. 71, pp. 1–15, 2022.
- [13] H.-Y. Zhou, J. Guo, Y. Zhang, X. Han, L. Yu, L. Wang, and Y. Yu, "nnformer: Volumetric medical image segmentation via a 3d transformer," *IEEE Transactions on Image Processing*, vol. 32, pp. 4036–4045, 2023.
- [14] A. Dosovitskiy, L. Beyer, A. Kolesnikov, D. Weissenborn, X. Zhai, T. Unterthiner, M. Dehghani, M. Minderer, G. Heigold, S. Gelly, J. Uszkoreit, and N. Houlsby, "An image is worth 16x16 words: Transformers for image recognition at scale," in *International Conference on Learning Representations*, 2021.
- [15] A. Gu, K. Goel, and C. R'e, "Efficiently modeling long sequences with structured state spaces," *ArXiv*, vol. abs/2111.00396, 2021.
- [16] A. Gu and T. Dao, "Mamba: Linear-time sequence modeling with selective state spaces," 2024.
- [17] L. Zhu, B. Liao, Q. Zhang, X. Wang, W. Liu, and X. Wang, "Vision mamba: Efficient visual representation learning with bidirectional state space model," *ArXiv*, vol. abs/2401.09417, 2024.
- [18] Y. Liu, Y. Tian, Y. Zhao, H. Yu, L. Xie, Y. Wang, Q. Ye, and Y. Liu, "Vmamba: Visual state space model," *ArXiv*, vol. abs/2401.10166, 2024.
- [19] Z. Liu, Y. Lin, Y. Cao, H. Hu, Y. Wei, Z. Zhang, S. Lin, and B. Guo, "Swin transformer: Hierarchical vision transformer using shifted windows," in *2021 IEEE/CVF International Conference on Computer Vision (ICCV)*, pp. 9992–10002, 2021.
- [20] Z. Wang, J.-Q. Zheng, Y. Zhang, G. Cui, and L. Li, "Mamba-unet: Unet-like pure visual mamba for medical image segmentation," *ArXiv*, vol. abs/2402.05079, 2024.
- [21] J. Ruan and S. Xiang, "Vm-unet: Vision mamba unet for medical image segmentation," *ArXiv*, vol. abs/2402.02491, 2024.
- [22] M. Zhang, Y. Yu, L. Gu, T. Lin, and X. Tao, "Vm-unet-v2 rethinking vision mamba unet for medical image segmentation," 2024.
- [23] S. Woo, J. Park, J.-Y. Lee, and I. S. Kweon, "Cbam: Convolutional block attention module," in *Computer Vision – ECCV 2018* (V. Ferrari, M. Hebert, C. Sminchisescu, and Y. Weiss, eds.), (Cham), pp. 3–19, Springer International Publishing, 2018.
- [24] J. Fu, J. Liu, H. Tian, Z. Fang, and H. Lu, "Dual attention network for scene segmentation," *2019 IEEE/CVF Conference on Computer Vision and Pattern Recognition (CVPR)*, pp. 3141–3149, 2018.
- [25] Q. Hou, D. Zhou, and J. Feng, "Coordinate attention for efficient mobile network design," in *2021 IEEE/CVF Conference on Computer Vision and Pattern Recognition (CVPR)*, pp. 13708–13717, 2021.
- [26] J. Park, S. Woo, J.-Y. Lee, and I.-S. Kweon, "Bam: Bottleneck attention module," *ArXiv*, vol. abs/1807.06514, 2018.
- [27] D. Misra, T. Nalamada, A. U. Arasanipalai, and Q. Hou, "Rotate to attend: Convolutional triplet attention module," in *2021 IEEE Winter Conference on Applications of Computer Vision (WACV)*, pp. 3138–3147, 2021.
- [28] F. Chollet, "Xception: Deep learning with depthwise separable convolutions," *2017 IEEE Conference on Computer Vision and Pattern Recognition (CVPR)*, pp. 1800–1807, 2016.
- [29] Z. Zhou, M. M. Rahman Siddiquee, N. Tajbakhsh, and J. Liang, "Unet++: A nested u-net architecture for medical image segmentation," in *Deep Learning in Medical Image Analysis and Multimodal Learning for Clinical Decision Support* (D. Stoyanov, Z. Taylor, G. Carneiro, T. Syeda-Mahmood, A. Martel, L. Maier-Hein, J. M. R. Tavares, A. Bradley, J. P. Papa, V. Belagiannis, J. C. Nascimento, Z. Lu, S. Conjeti, M. Moradi, H. Greenspan, and A. Madabhushi, eds.), (Cham), pp. 3–11, Springer International Publishing, 2018.
- [30] O. Oktay, J. Schlemper, L. L. Folgoc, M. J. Lee, M. P. Heinrich, K. Misawa, K. Mori, S. G. McDonagh, N. Y. Hammerla, B. Kainz, B. Glocker, and D. Rueckert, "Attention u-net: Learning where to look for the pancreas," *ArXiv*, vol. abs/1804.03999, 2018.
- [31] Y. Gao, M. Zhou, D. Liu, and D. N. Metaxas, "A multi-scale transformer for medical image segmentation: Architectures, model efficiency, and benchmarks," *ArXiv*, vol. abs/2203.00131, 2022.
- [32] Y. Peng, M. Sonka, and D. Z. Chen, "U-net v2: Rethinking the skip connections of u-net for medical image segmentation," *ArXiv*, vol. abs/2311.17791, 2023.
- [33] Y. Zhang, H. Liu, and Q. Hu, "Transfuse: Fusing transformers and cnns for medical image segmentation," in *Medical Image Computing and Computer Assisted Intervention – MICCAI 2021: 24th International Conference, Strasbourg, France, September 27–October 1, 2021, Proceedings, Part I*, (Berlin, Heidelberg), p. 14–24, Springer-Verlag, 2021.
- [34] S. Hu, Z. Liao, and Y. Xia, "Devil is in channels: Contrastive single domain generalization for medical image segmentation," in *Medical Image Computing and Computer Assisted Intervention – MICCAI 2023* (H. Greenspan, A. Madabhushi, P. Mousavi, S. Salcudean, J. Duncan, T. Syeda-Mahmood, and R. Taylor, eds.), (Cham), pp. 14–23, Springer Nature Switzerland, 2023.
- [35] E. K. Aghdam, R. Azad, M. Zarvani, and D. Merhof, "Attention swin unet: Cross-contextual attention mechanism for skin lesion segmentation," in *2023 IEEE 20th International Symposium on Biomedical Imaging (ISBI)*, pp. 1–5, 2023.

- [36] N. C. F. Codella, D. Gutman, M. E. Celebi, B. Helba, M. A. Marchetti, S. W. Dusza, A. Kalloo, K. Liopyris, N. Mishra, H. Kittler, and A. Halpern, "Skin lesion analysis toward melanoma detection: A challenge at the 2017 international symposium on biomedical imaging (isbi), hosted by the international skin imaging collaboration (isic)," in *2018 IEEE 15th International Symposium on Biomedical Imaging (ISBI 2018)*, pp. 168–172, 2018.
- [37] N. C. F. Codella, V. M. Rotemberg, P. Tschandl, M. E. Celebi, S. W. Dusza, D. Gutman, B. Helba, A. Kalloo, K. Liopyris, M. A. Marchetti, H. Kittler, and A. C. Halpern, "Skin lesion analysis toward melanoma detection 2018: A challenge hosted by the international skin imaging collaboration (isic)," *ArXiv*, vol. abs/1902.03368, 2019.
- [38] D.-P. Fan, G.-P. Ji, T. Zhou, G. Chen, H. Fu, J. Shen, and L. Shao, "Pranet: Parallel reverse attention network for polyp segmentation," in *Medical Image Computing and Computer Assisted Intervention – MICCAI 2020: 23rd International Conference, Lima, Peru, October 4–8, 2020, Proceedings, Part VI*, (Berlin, Heidelberg), p. 263–273, Springer-Verlag, 2020.
- [39] D. Jha, P. H. Smedsrud, M. A. Riegler, P. Halvorsen, T. de Lange, D. Johansen, and H. D. Johansen, "Kvasir-seg: A segmented polyp dataset," in *MultiMedia Modeling* (Y. M. Ro, W.-H. Cheng, J. Kim, W.-T. Chu, P. Cui, J.-W. Choi, M.-C. Hu, and W. De Neve, eds.), (Cham), pp. 451–462, Springer International Publishing, 2020.
- [40] J. Bernal, F. J. Sánchez, G. Fernández-Esparrach, D. Gil, C. Rodríguez, and F. Vilariño, "Wm-dova maps for accurate polyp highlighting in colonoscopy: Validation vs. saliency maps from physicians," *Computerized Medical Imaging and Graphics*, vol. 43, pp. 99–111, 2015.
- [41] N. Tajbakhsh, S. R. Gurudu, and J. Liang, "Automated polyp detection in colonoscopy videos using shape and context information," *IEEE Transactions on Medical Imaging*, vol. 35, no. 2, pp. 630–644, 2016.
- [42] D. Vázquez, J. Bernal, F. J. Sánchez, G. Fernández-Esparrach, A. M. López, A. Romero, M. Drozdal, and A. C. Courville, "A benchmark for endoluminal scene segmentation of colonoscopy images," *CoRR*, vol. abs/1612.00799, 2016.
- [43] D. Jha, S. Ali, K. Emanuelsen, S. A. Hicks, V. Thambawita, E. Garcia-Ceja, M. A. Riegler, T. de Lange, P. T. Schmidt, H. D. Johansen, D. Johansen, and P. Halvorsen, "Kvasir-instrument: Diagnostic and therapeutic tool segmentation dataset in gastrointestinal endoscopy," in *MultiMedia Modeling* (J. Lokoč, T. Skopal, K. Schoeffmann, V. Mezaris, X. Li, S. Vrochidis, and I. Patras, eds.), (Cham), pp. 218–229, Springer International Publishing, 2021.
- [44] I. Loshchilov and F. Hutter, "Decoupled weight decay regularization," in *International Conference on Learning Representations*, 2017.
- [45] I. Loshchilov and F. Hutter, "SGDR: stochastic gradient descent with warm restarts," in *5th International Conference on Learning Representations, ICLR 2017, Toulon, France, April 24-26, 2017, Conference Track Proceedings*, OpenReview.net, 2017.